Time Resolved in Situ XAFS Study of the Electrochemical Oxygen Intercalation in SrFeO$_{2.5}$ Brownmillerite Structure: Comparison with the Homologous SrCoO$_{2.5}$ System[†]

Andrea Piovano,[‡,§] Giovanni Agostini,[‡] Anatoly I. Frenkel,[∥] Tanguy Bertier,[‡,§] Carmelo Prestipino,[§] Monica Ceretti,[§] Werner Paulus,[§] and Carlo Lamberti*,[‡]

Department of Inorganic, Physical and Materials Chemistry, INSTM Reference Center and NIS Centre of Excellence, Università di Torino, Via P. Giuria 7, I-10125 Torino, Italy, Sciences Chimiques de Rennes - UMR 6226, Matériaux Inorganiques: Chimie Douce et Réactivité, Université de Rennes 1, Campus de Beaulieu, Bât 10B, F-35042 Rennes, France, and Department of Physics, Yeshiva University, New York, New York 10016, United States

Low temperature oxygen ionic conductors are key materials for the development of the next generation solid oxide fuel cells. In this regard, SrMO$_{2.5}$ (M = Fe,Co) systems with a Brownmillerite-type structure are able to reversibly intercalate oxygen in an electrochemical reaction at room temperature to reach SrMO$_3$ stoichiometry. To understand and characterize this behavior, at the atomic level, in situ X-ray absorption spectroscopy experiments during the electrochemical oxidation reaction were performed for both SrFeO$_{2.5}$ and SrCoO$_{2.5}$ compounds at the Fe and Co K-edge, respectively. The comparative analysis of the two experiments allowed us to emphasize the similarities and differences observed during electrochemical oxidation of the two parent compounds. The data were analyzed both in XANES and EXAFS regions to extract both electronic configuration and local order information. To extract as much information as possible from collected data, the standard linear combination of spectra was complemented by the principal component analysis advanced method, which allowed us to clarify some aspects of the reaction process that were otherwise hidden. As for SrCoO$_{2.5+x}$ ordered intermediates (x = 0.25, 0.375) that could have been identified by neutron diffraction and XAFS experiments [*J. Am. Chem. Soc.* **2006**, *128*, 13161], no ordered intermediates of the homologous SrFeO$_{2.5+x}$ different from an oxygen deficient perovskite phase have been reported to occur during the oxygen intercalation reaction, except on a very local level. However, a detailed fit of the EXAFS signals for starting and final phases showed that the final fully oxidized compound (with stoichiometry SrCoO$_3$) has been obtained for SrCoO$_{2.5}$, whereas for SrFeO$_{2.5}$, the reaction ended before the expected charge transfer. We interpret the formation of SrFeO$_3$ to be accompanied by the parasitic formation of an unknown phase, containing Fe(III). Furthermore we were able to highlight that, at a local level, the most probable space group for SrCoO$_{2.5}$ at ambient temperature is *Imma*, as the average local environments extracted from *Pnma* and *I2mb* models were not able to reproduce the experimental EXAFS spectrum.

1. Introduction

Transition-metal oxides exhibiting mixed electronic/ionic conductivity are materials of high interest for their potential application as electrodes in solid oxide fuel cells (SOFCs) or batteries,[1–12] sensors,[13–16] magnetic recording,[17] membranes for oxygen separation,[18,19] catalysts,[20–23] and photocatalysis.[24]

Focusing on the applications for SOFCs and batteries, a huge scientific work was performed in the past decade in order to understand the problems related to oxygen mobility in solid materials.[1–12,25–30] Among them, high operating temperatures are required for oxygen ions conduction, making application for fuel cells rather limited.[31] Oxygen ion conductors at low temperatures are thus the key material for future technologies, and in this direction, the electrochemical intercalation of oxygen into Brownmillerite type defective perovskite SrMO$_{2.5}$ (M = Co, Fe) at ambient temperature[3,25] has to be seen has a fundamental step. Actually these two compounds are the only known systems so far showing high oxygen ion conduction at room temperature with a huge charge transfer of one electron per formula unit (e$^-$/f.u.). Formally the reaction, which is carried out in an aqueous alkaline electrolyte, can be described as given in eq 1

$$SrMO_{2.5} + xO^{2-} \leftrightarrow SrMO_{2.5+x} + 2xe^-$$
$$(0 < x < 0.5)\ (M = Co, Fe) \quad (1)$$
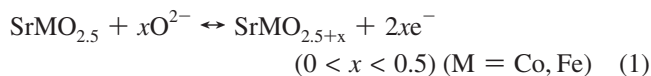
The fast reaction kinetics for the oxidation from the Brownmillerite phase SrMO$_{2.5}$ (containing 1D channels of oxygen vacancies) to the fully oxidized perovskite phase SrMO$_{3.0}$ allows us to perform the electrochemical oxidation reaction within a few days under equilibrium conditions in a controlled way (the reaction speed being tuned by the applied current value), opening the possibility to follow in situ the complete oxidation reaction as a function of the oxygen stoichiometry. Structural investigations of the SrCoO$_{2.5}$ → SrCoO$_{3.0}$ transformation observed by in situ neutron and XAFS methods,[3] have shown the formation of several intermediate phases, and a non linear evolution of

the Co valence state from Co^{3+} to Co^{4+}, allowing us to monitor the complexity of low temperature solid state reaction mechanisms and suggesting the transient formation of O^- species. In this regard, it is worth mentioning the recent DFT study (SLDA approximation) by Tapilin et al.,[32] who investigated the electronic structures of $SrCoO_x$ (x = 3, 2.875, and 2.75). Two kinds of oxygen vacancy ordering, more stable than the random vacancy distribution were revealed.

Electrochemical oxygen intercalation at low temperature into $SrFeO_{2.5}$ structure has been so far investigated in situ by X-ray diffraction by Nemudry et al.,[25] where the presence of intermediate phases such as $SrFeO_x$ (with x = 2.75, 2.875) has been claimed. Their structural identification via X-ray diffraction was, however, difficult as no corresponding diffraction peaks were found related to the enlarged unit cell and also the orthorhombic splitting expected in the case of $SrFeO_{2.75}$ was more perceived as a line broadening rather than a clear separation of diffraction peaks. Evidence of ordered intermediates came, however, from Mössbauer spectroscopy and electron microscopy.[25] Moreover the oxygen intercalation into $SrFeO_{2.5}$ appears to be much more complex compared to $SrCoO_{2.5}$, due to the appearance of extra peaks found in situ by XRD diffraction, which can not be attributed to the cubic $SrFeO_3$ and which do remain unexplained so far.

To shed light on this subject, we decided to reinvestigate, using X-ray absorption spectroscopy (XAS), the oxygen intercalation reaction, already studied by Nemudry et al.[25] with XRPD. As already proven for the $SrCoO_{2.5}$ system,[3] the combined use of complementary methods such as diffraction and XAS, sensible to long and short-range order respectively may be highly informative. We thus used here in situ XAS, to investigate on a more local level the intercalation of oxygen into $SrFeO_{2.5}$, in order to identify or not whether the intermediate phases mentioned above could be observed and correspond to the phases described by Hodge et al.[33] In this work XAS results, collected at the Fe K-edge for $SrFeO_{2.5}$ system, are reported and compared to the previous data collected on $SrCoO_{2.5}$ at the Co K-edge.[3] This parallelism permits a comparison of the behavior of these two parent compounds and to highlight similarities and differences in the evolution of the oxidation state of the two 3d metal as a function of the charge transfer along the electrochemical reaction 1.

2. Experimental and Methods

2.1. Materials. $SrFeO_{2.5}$ and $SrCoO_{2.5}$ samples were both prepared via solid-state reaction. $SrFeO_{2.5}$ was obtained starting from a thorough mixing in stoichiometric quantities of $SrCO_3$ and Fe_2O_3, which was then heated in air at 1273 K for 24 h and afterward ground and pressed into pellets of about 1 g weight and 13 mm diameter. Pellets were heated in air for 48 h at 1273 and 1473 K successively. Finally, to reach the final exact stoichiometry, the pellets were heated again at 1473 K, slowly cooled under vacuum, and then quenched in liquid nitrogen. $SrCoO_{2.5}$ preparation starts from a thorough mixture of $SrCO_3$ and Co_3O_4 in stoichiometric quantities, which was then ground and pressed into 13 mm diameter 1 g weight pellets. Pellets were heated in air for 48 h at 1173 and 1523 K successively. To reach the exact final stoichiometry, a further annealing at 1273 K for 6 h was performed. At this temperature the phase still has cubic symmetry, and in order to induce the transformation to the orthorhombic Brownmillerite-type structure, a fast quenching into liquid N_2 was carried out.[3] For comparison $SrFeO_{3.0}$ and $SrCoO_{3.0}$ model compounds have been measured under static (not electrochemical) conditions. They
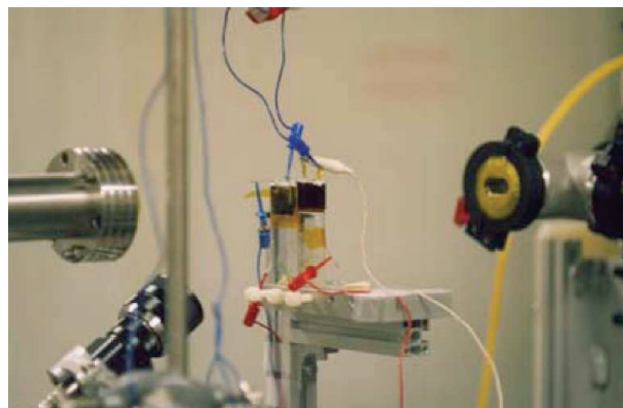

Figure 1. Photograph reporting the in situ electrochemical setup, mounted inside BM29, and allowing to follow with X-ray absorption spectroscopy the $SrMO_{2.5} + xO^{2-} \leftrightarrow SrMO_{2.5+x} + 2xe^-$ ($0 < x < 0.5$) (M = Co, Fe) reaction.

have been oxidized in Rennes-1 laboratories from the as obtained $SrMO_{2.5}$ pellets via electrochemical oxidation in 1 N KOH electrolyte and checked by XRPD.

2.2. X-ray Absorption Data Collection. Time resolved X-ray absorption experiments were performed at the Fe and Co K-edges on $SrFeO_{2.5}$ and $SrCoO_{2.5}$ systems, respectively, in transmission mode at the ESRF BM29 beamline.[34] In both cases a double crystal Si(111) monochromator was used, while harmonic rejection was made using mirrors or by detuning the monochromator crystal in the Fe and Co cases, respectively. In order to guarantee an exact energy calibration, the following experimental setup has been adopted: (i) a first ionization chamber measures the intensity of the incoming monochromatic beam $I_0(E)$; (ii) the beam was partially absorbed passing the sample of optimized thickness x (about 25 μm); (iii) a second ionization chamber measures the intensity of the transmitted beam $I_1(E)$; (iv) downstream of the second chamber the beam was further absorbed passing through a reference metal foil (Fe or Co depending on the case) of thickness x_R; (v) finally, the beam transmitted by the reference foil was measured by a third ionization chamber $I_2(E)$. In this way, the absorption coefficients for the sample (μ) and the reference (μ_R) were measured at the same time, for a given energy selected by the monochromator, applying the classical law of transmission phenomena: $\mu(E)x = \ln[I_0(E)/I_1(E)]$ and $\mu_R(E)x_R = \ln[I_1(E)/I_2(E)]$.[35] Then, small fluctuations in the angle/energy relationship of the monochromator, due to thermal instabilities of the silicon crystals and beam fluctuations, can be, if needed, corrected a posteriori. These checks are of fundamental importance when the evolution of the oxidation state of a transition metal during a redox reaction has to be followed. Measurements were performed in situ in an electrochemical cell containing three electrodes (working electrode, Pt counter electrode and Ag/AgCl reference electrode) and optimized to minimize the thickness of the electrolyte, which is highly absorbing at the Fe or Co K-edges (Figure 1). In this regard a 1 N NaOH electrolyte was adopted for the Fe K-edge experiment, in order to limit the absorption of the solution which is strong at the employed range of energies, while 1 N KOH was employed for the Co K-edge experiment. During the electrochemical reaction, performed in galvanostatic mode, i.e., applying a constant current, the current density was kept below 500 μA/cm^2 on each sample.

The pellets used for in situ electrochemical reaction were prepared by intimate mixing of polycrystalline sample ($SrFeO_{2.5}$ or $SrCoO_{2.5}$) powders with 2% Teflon and then pressed into homogeneous electrodes of desired thickness. In both cases, the

pellets homogeneity was checked by monitoring the transmitted beam upon scanning the sample in a beam sharply defined by closing both horizontal and vertical secondary slits.

For both edges, the X-ray absorption near-edge structure (XANES) region was sampled with 0.3 eV steps, while the extended X-ray absorption fine structure (EXAFS) region was acquired up to 13 Å^{-1} with a constant sampling step, in k space, of 0.025 Å^{-1}. With this configuration, but slightly different integration times, a single X-ray absorption spectrum require something more than 35 min at the Fe K-edge and slightly less than 40 min at the Co K-edge, both including high resolution XANES and EXAFS and the time needed to move the monochromator back below the edge for the next scan. In any case, current was set in order to have the complete oxidation reaction in about 2500 min. In this way, roughly 70 (60) spectra were collected at the Fe (Co) K-edge. Within a single spectrum the charge transfer n was 0.014 (0.016) e$^-$/f.u., corresponding to $\Delta x = 0.007$ (0.008), a sufficiently low value to consider the sample almost unchanged between the first and last point of every single spectrum.

2.3. EXAFS and XANES Data Analyses. Treatment of the raw X-ray absorption data was performed with Athena package,[36] allowing the alignment, normalization, $\chi(k)$ extraction, as well as the linear combination analysis of the experimental data. Eventual narrow glitches were removed at this stage. During this preprocessing of the data the extraction edge position E_0 was defined as the maximum derivative of the μx spectrum and recalibrated with the reference $\mu_R x$ spectrum if needed. In this way edge shift due to transformation of species during reaction can be quantified. EXAFS data analysis was performed using the Artemis software.[36] This package computes phases and amplitudes functions for both single scattering (SS) and multiple scattering (MS) paths exploiting FEFF6 code[37] and performs nonlinear least-squares fit of the theory to the data. The validity of such phases and amplitudes has been checked on SrFeO$_{2.5}$ and SrCo$_{3.0}$ model compounds, using as input the corresponding structures solved by powder diffraction.[3]

As discussed in section 2.2, the in situ X-ray absorption experiments had generated a large number of progressive spectra. The evolution of the oxygen intercalation reaction 1 has been followed by simulating the ith spectrum of the series as the linear combination of the last ($i = 70$) [$\chi^{Ox}(k_j)$] and the first [$\chi^{Red}(k_j)$] ($i = 1$) spectrum of the series, corresponding to the SrMO$_{2.5}$ brownmillerite phase

$$\chi_i^{Theo}(k_j, x_{i,}^{Red} y_i^{Ox}) = x_i^{Red}\chi^{Red}(k_j) + y_i^{Ox}\chi^{Ox}(k_j) \qquad (2)$$

where k_j ($j = 1, 2, 3, ..., N$) are the k values where the experimental spectra have been sampled and x_i^{Red} and y_i^{Ox} are fraction of the starting and final phase, respectively. The latter two parameters are optimized by standard least-squares methods, minimizing the $F(x_i^{Red}, y_i^{Ox})$ defined as

$$F(x_i^{Red}, y_i^{Ox}) = \sum_{j=1}^{N} [\chi_i^{exp}(k_j) - \chi^{Theo}(k_j, x_i^{Red}, y_i^{Ox})]^2 \qquad (3)$$

We are thus dealing with a two parameter fit, where the sum of the fractions x_i^{Red} and y_i^{Ox} is not forced to be equal to 1.0. This means consequently, that a significant deviation of $x_i^{Red} + y_i^{Ox}$ from 1.0, accompanied by a decrease of the quality of the fit would imply that the two phase model is not adequate for the reproduction of the experimental data. The same approach

has been applied to the sequence of XANES spectra. For both materials the fit was performed in the XANES region around absorption edge (from 20 eV before to 30 eV above) and in the EXAFS one (k space in the 2−12 Å^{-1} interval).

Principal component analysis (PCA) is a useful statistical technique to find patterns on data of high dimensions. In particular it is able to find the most important components contributing to all of the data sets and represent all of these data as a linear combination of only these components. With this method it is then a simple procedure to recognize the presence of the two or more phases during a reaction, if a sufficient contrast among different spectra is present.[38−42] Furthermore, being a linear algebra based method, it is exempt from the model-based assumptions on chemical nature or structure of the phases. The change from the use of abstract components to real chemical species, or phases, can be performed in by a target transformation procedure rotating the basis of the abstract components to the new basis of suitable reference compounds. In our work we employed the PCA package developed by Wasserman.[39]

3. Results

X-ray absorption technique, due to its atomic selectivity and high sensitivity to the oxidation state and local order around absorber, has been widely employed so far to analyze the structure and electronic behavior of a variety of metal and mixed metal oxides becoming a standard approach for this class of materials.[3,6−10,21,22,35,43−76] The high packing of such materials and their long-range order often results in complex EXAFS signals characterized by the superimposition of a high number of SS and MS signals resulting in constructive components up to 6−8 Å from the adsorbing atom.[3,53,65] Notwithstanding this complexity, the knowledge of the long-range order from diffraction studies makes the reconstruction of the EXAFS signal straightforward. Exception is given when the space group of the solid is not unambiguously known. This is the case of mixed oxides with Brownmillerite AMO$_{2.5}$ structure; Brownmillerite exhibits an alternation of MO$_6$ octahedra layers with MO$_4$ tetrahedra ones. While MO$_6$ octahedra can not show any preferred orientation, the MO$_4$ tetrahedra do. Depending on the relative orientation of MO$_4$ tetrahedral chains, the AMO$_{2.5}$ structure can belong to *Pnma*, *Imma*, or *I2mb* space groups.[3] The general problem lies in the fact that only slight differences exist in the arrangement of the MO$_4$ tetrahedral chains for these three space groups. *I2mb* and *Pnma* refer to two different ordering schemes for the MO$_4$ chains, whereas *Imma* implies a statistical disorder of MO$_4$ tetrahedra, which is approximately equivalent to a coherent mixing of *Pnma* and *I2mb* domains.[3] Note that also a dynamically disordered structure has recently been proposed in the SrFeO$_{2.5}$ case.[29] Other complex situations arise when a mixture of phases is present in the sample, either for heterogeneity reasons or because the study implies a dynamical (time-resolved) investigation of a solid state phase transition.[3,6−10,70,75,76]

In such cases, due to the complexity of the structure, the interpretation of the EXAFS spectra is not a simple task, and standard data treatments could not be sufficient to face the complex structural problem. The in situ investigation of oxygen intercalation via electrochemical reaction, see eq 1, clearly belongs to this category, because (i) the starting materials, both SrFeO$_{2.5}$ and SrCoO$_{2.5}$, belong to the Brownmillerite family showing structural disorder and (ii) a complex solid state phase transformation is occurring.[3,25] Due to the importance of extracting as detailed as possible reaction information, including
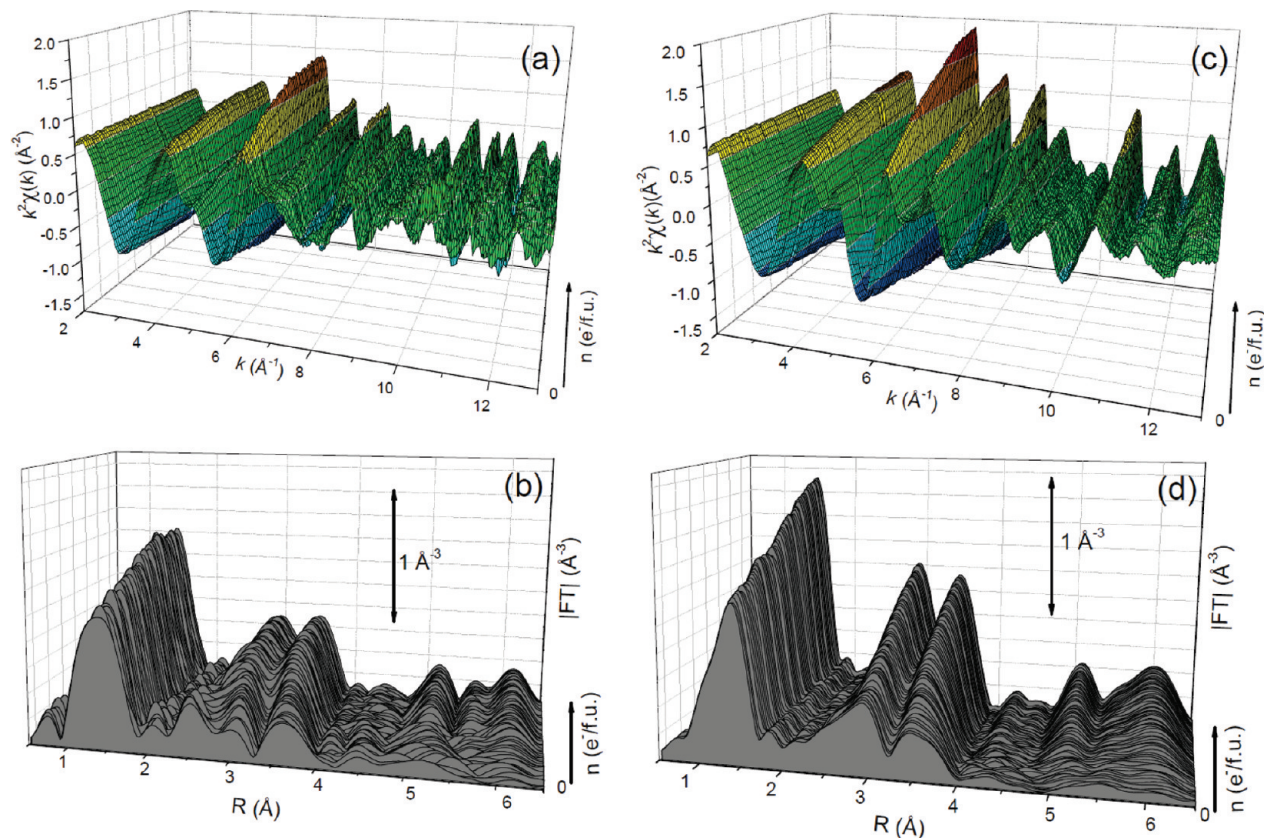
Figure 2. Evolution of the EXAFS spectra along the in situ electrochemical oxidation reaction (extracted from absorption data reported in Figure 3). Panels a and b refer to the Fe K-edge experiment and panels c and d to the Co K-edge one. Panels a and c report, in k-space, the $k^2\chi(k)$ functions in the $2-12.5$ Å^{-1} range. Panels b and d report the phase uncorrected Fourier transform magnitudes of the $k^2\chi(k)$ functions.

the presence of eventual intermediate or extra phases, a combination of standard methods and more advanced techniques have to be applied in the data treatment. In this contribution, the standard method of combining linearly initial and final XANES and EXAFS spectra[3,62,77−79] is complemented by the PCA approach[40,41,70,80−82] with the aim of extracting the different contributions in the spectra during the reaction process and obtaining a cross validation of results.

The $k^2\chi(k)$ functions reported in Figure 2a,c show an evident increase in the intensities along the oxidation reaction. This evidence is associated with the increase in the average coordination number around the absorber occurring during oxygen intercalation, which progressively transforms half of the M atoms initially in the 4-fold-coordination to 6-fold-coordinated cations. In this regard, even more important is the increase in the degree of order as compounds are going from a partially disordered starting phase to a final phase showing cubic symmetry, where the higher symmetry causes an increase of degeneration of the scattering paths that at the end interfere fully constructively. The Fourier transform (FT) of the k^2-weighted $\chi(k)$ spectra (Figure 2b,d) clearly supports what was discussed above in terms of the increase in the first coordination shell along the oxidation experiments. Even more relevant is the fact that the EXAFS signal of both starting phases exhibits well-defined contributions up to 4 Å only, whereas at higher R values no contribution is observed above the noise level. As the oxidation proceeds, the three peaks in the $0.7-4.0$ Å range increase their amplitude in parallel to the appearance of new and well-defined features in the $4.5-6.6$ Å region. These observations directly proves the progressive improvement of the local order of the structure around the absorber.

Even more informative is Figure 3a,b where normalized absorption spectra of SrFeO$_{2.5+x}$ and SrCoO$_{2.5+x}$ systems, panels a and b, respectively, during their respective electrochemical oxidation process are shown. The main part of Figure 3a,b represents the XANES region ($7110-7150$ eV for the Fe K-edge, $7705-7750$ eV for the Co one), whereas the top insets emphasize the pre-edge peak transformation and the bottom ones reproduce the respective extended region of the normalized absorption coefficient data. In every layer the initial phase with oxygen stoichiometry $x = 2.5$ is reported as a red curve, whereas the final oxidized phase (obtained after a formal electron charge transfer of $n = 1.0$ e$^-$/f.u.) is shown as a black one. A selection of intermediate spectra is depicted with pale gray curves allowing to appreciate the progressive solid state transformation, eq 1.

An inspection of the whole set of spectra for both experiments makes possible to point out important changes in the absorption profiles and intensities. In particular, the most important variation is experienced by the edge position that blue-shifts during electrochemical oxidation by 1.2 eV at the Fe K-edge and by 2.0 eV at the Co K-edge, following the progressive evolution form M(III) species toward M(IV) ones ($M =$ Fe, Co). Furthermore, we observe the progressive increase of the white-line intensity (I_{W-L}), associated with the increase of the average coordination number around absorbing atom during oxygen intercalation.[83] The final increase in I_{W-L} turns out to be of 0.08 and 0.16 normalized μx units for the Fe and Co experiment, respectively. The pre-edge feature in the region of the dipole-forbidden 1s → 3d transition is evident in both starting compounds, and in general, it shifts toward higher energies during reaction (Figure 3a,b, top insets).[84,85] However in the Fe

Oxygen Intercalation in SrFeO2.5

J. Phys. Chem. C, Vol. 115, No. 4, 2011 **1315**

TABLE 1: Summary of the Parameters Optimized in the EXAFS Fit of the Starting ($SrFeO_{2.5}$ and $SrCoO_{2.5}$) Brownmillerite Phases and Perovskite Final Phases ($SrFeO_{3.0-\delta}$ and $SrCoO_{3.0}$), Representing the First and the Last Spectra of the Series Reported in Figure 2b,d[a]

nominal sample stoichiometry	space group	site and occupancy	ΔE_0 (eV)	S_0^2	α	σ_1^2 (Å²)	R_{factor}
$SrFeO_{2.5}$	*Pnma*	O_h (0.5)	-2 ± 1	0.43 ± 0.07	-0.005 ± 0.009	0.0052	0.135
		T_d (0.5)	-3 ± 2			0.0052	
$SrFeO_{3.0-\delta}$	*Pm-3m*	O_h ($1.0-0.5\delta$)	-2.5 ± 1.0	0.45 ± 0.04	$+0.001 \pm 0.003$	0.0063 ± 0.0009	0.052
$SrFeO_{3.0}$	*Pm-3m*	O_h (1.0)	-3.5 ± 1.0	0.47 ± 0.04	-0.001 ± 0.002	0.0052 ± 0.0007	0.041
$SrCoO_{2.5}$	*Pnma*	O_h (0.5)	$+6.0 \pm 2.5$	0.52 ± 0.09	0.025 ± 0.015	0.0052	0.285
		T_d (0.5)	-6.0 ± 1.5			0.0052	
$SrCoO_{2.5}$	*I2mb*	O_h (0.5)	13 ± 4	$0.30 \pm 0,09$	0.04 ± 0.01	0.0052	0.458
		T_d (0.5)	3 ± 1			0.0052	
$SrCoO_{3.0}$	*Pm-3m*	O_h (1.0)	-2 ± 1	0.57 ± 0.05	-0.000 ± 0.003	0.0052 ± 0.0008	0.052

[a] In all cases the fit was performed in R space (from 1.0 to 4.2 Å), on the k^2-weighted FT of the $\chi(k)$ function transformed in the $\Delta k = 2-12$ Å^{-1}, resulting in a number of independent parameters $N > 20$. For the cubic perovskite phases only one O_h adsorbing site is present. For the Brownmillerite phases both O_h and T_d contributions have been considered, weighted by 50% each. For the $SrFeO_{2.5}$ case reasonable (and equivalent) fits were obtained assuming both *Pnma* and *I2mb* space groups, only the former being reported. Conversely, this approach failed for the $SrCoO_{2.5}$ case, where both *Pnma* and *I2mb* models were not able to reproduce the experimental spectrum. Nonoptimized parameters can be recognized by the absence of the corresponding error bar. All fits run over only 4 independent parameters, so that the relative goodness factors R_{factor} can be directly compared. See Figure 4 to appreciate the quality of the fits in R-space.

containing sample, the pre-edge feature blue-shifts by about 0.4 eV only and remains structured even if broadened and less intense, whereas in Co, the feature blue-shifts by more than 0.7 eV and loses its structure becoming completely broad. All of this evidence suggests that the $SrMO_{2.5} \rightarrow SrMO_{3.0}$ reaction is complete for the Co case, while it is not in the Fe case. The direct proof of this interpretation comes by comparing the final XANES spectra of the in situ reactions (black curves) with those of the $SrFeO_{3.0}$ and $SrCoO_{3.0}$ model compounds (blue scattered curves in Figure 3). Two simples hypotheses are able to explain the nonideal behavior of the oxygen intercalation reaction in the $SrFeO_{2.5}$ case. The first is that the sample does not reach the final oxidation, stopping uniformly the reaction at a $SrFeO_{3.0-\delta}$ level. The second is that only a fraction of the sample reaches the $SrFeO_{3.0}$ final level, whereas in the complementary fraction iron stays in the initial (III) oxidation state. To discriminate among these two possibilities, a detailed analysis of the experimental data will be needed. In the following we will refer to the sample obtained at the end of the oxidation $SrFeO_{2.5}$ as sample $SrFeO_{3.0-\delta}$.

4. Discussion

4.1. Standard Methods. An inspection of the extended region above the absorption edge (insets of Figure 3a,b) shows the presence of a number of possible isosbestic points, which in principle can represent a direct transformation from phase A to phase B.[3,62,86] In such cases, the application of a standard linear combination fit between initial and final phases, both on the XANES and EXAFS parts of the X-ray absorption spectrum, can directly point out the fraction of starting and final materials present at each step of the transformation. However, to validate the results, the nature of the starting and final phases must be verified. A way to do this check is to perform a standard analysis of the corresponding EXAFS spectra.[3,62,78,87]

4.1.1. Validation of Starting and Final Phases by EXAFS. To verify that the experimental spectra collected on the starting ($SrFeO_{2.5}$ and $SrCoO_{2.5}$) and final ($SrFeO_{3.0-\delta}$ and $SrCoO_{3.0}$) samples correspond well to the expected stoichiometries, we performed a fit of the corresponding EXAFS spectra using as input the structures obtained by diffraction studies.[3,25] For homogeneity reasons the simulations have been performed on all systems by reproducing the most relevant single scattering and multiple scattering paths within $R_{eff} < 4.2$ Å, where R_{eff} is half of the global path length and corresponding so to the bond

length for SS paths. All $k^2\chi(k)$ functions were Fourier transformed in the $2-12$ Å^{-1} interval, and the fit was performed in R-space in the $1.0-4.2$ Å range, resulting in a number of independent parameters larger than 20.

For the cubic perovskite ($SrFeO_{3.0}$ and $SrCoO_{3.0}$), only one independent O_h adsorbing site is present, so that the EXAFS fit was straightforward. In all cases just four parameters have been optimized: (i) a common energy shift of the adsorption edge ΔE_0; (ii) a common amplitude factor S_0^2; (iii) an isotropic expansion/compression parameter α that expands/contracts all scattering paths according to the equation: $R = R_0 + \alpha R_{eff}$; and (iv) an unique Debye−Waller factor that scales for all paths with the square root of R_{eff}: $\sigma^2 = \sigma_1^2 (R_{eff}/R_1)^{1/2}$, where σ_1^2 (R_1) is the Debye−Waller factor (bond distance) of the first shell Fe−O or Co−O SS path.[88−93]

The brownmillerite case is more complex, because in both *Pnma* and *I2mb* space groups 50% of the adsorbing atoms (Fe or Co) occupy the O_h site, whereas the remaining 50% are hosted in the T_d site. This implies that the overall EXAFS signal is due to the superimposition of two different signals. So, in principle, we should duplicate the fitting parameters (ΔE_0, S_0^2, α, and σ_1^2) for all SS and MS paths generated around the T_d site and weighting the families of paths belonging to O_h and T_d environments by a factor 0.5 each. Such an 8-parameter fit resulted in instabilities of the optimization procedure, yielding to high correlation among parameters and high errors associated to the fitted variables, which optimized values were significantly dependent by the starting guesses. We thus decided to reduce to four the number of optimized variables also in the case of the brownmillerite phases. This was done by (i) fixing both $\sigma_1^2(O_h)$ and $\sigma_1^2(T_d)$ to the $\sigma_1^2(O_h)$ value optimized on the cubic phase, (ii) assuming the same amplitude factor, $S_0^2(O_h) = S_0^2(T_d)$, (iii) the same isotropic expansion/compression parameter $\alpha(O_h) = \alpha(T_d)$ for both sites, and (iv) optimizing two independent ΔE_0. We are aware that this represents a very crude approximation, but the aim of this study is just to confirm, at the local ground, that the stating phases are actually the expected ones.

Table 1 shows the collection of optimized parameters obtained in the best fit procedures performed as described above, while the direct comparison between experimental and best theoretical curves is reported in Figure 4. Both $SrFeO_{3.0}$ and $SrCoO_{3.0}$ compounds were satisfactorily fitted with the simple 4-parameter model, with small ΔE_0, meaningful σ_1^2, and α values that
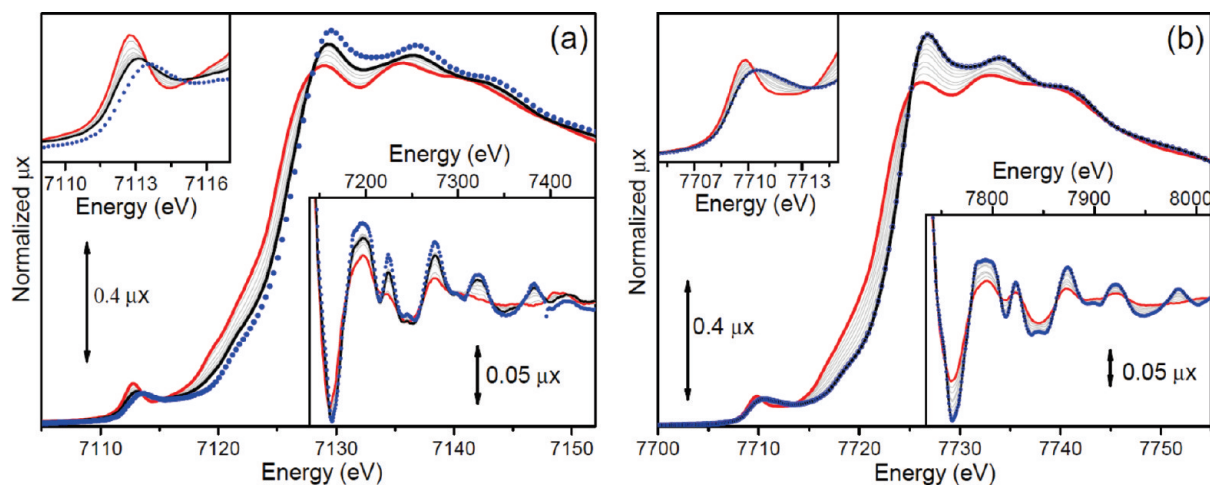
Figure 3. Normalized absorption coefficients (μx) reported in the XANES region across the Fe K-edge, part a, and across the Co K-edge, part b, during the in situ electrochemical oxidation process. Starting spectrum (red curve) corresponds to the phase with oxygen stoichiometry $x = 2.5$; final phase (black curve) corresponds to the highest oxidation state reached in these experiments; selection of intermediate curves (light gray lines), corresponding to intermediate stoichiometry. Also reported as blue scattered data are the XANES spectra of $SrFeO_{3.0}$ and $SrCoO_{3.0}$ model compounds. Top and bottom insets report a magnification of the XANES spectra in the $1s \rightarrow 3d$ transition region and a extended region above the edge, respectively.
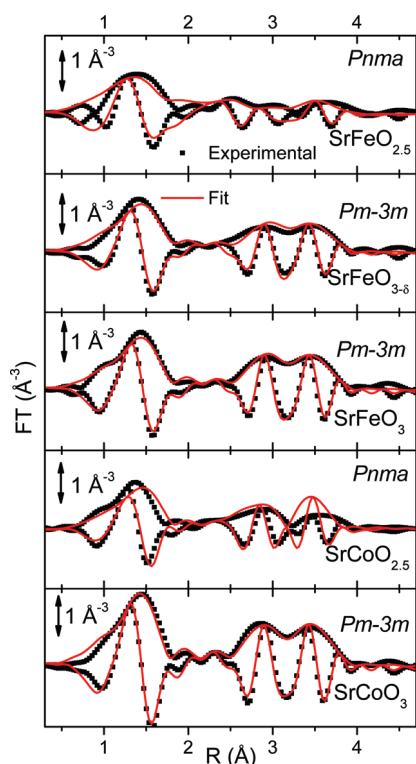

Figure 4. Graphical representation in R space (showing both moduli and imaginary parts) of the 4-parameter fits reported in Table 1. Experimental (scattered black squares) and best fit (continuous red curves).

confirm the XRPD structures within the error bars. The only unusual result is the low value obtained for S_0^2 that is expected to be usually in the $0.8-1.1$ range while we obtain 0.47 ± 0.04 and 0.57 ± 0.05 for the $SrFeO_{3.0}$ and $SrCoO_{3.0}$ system, respectively. Although rare, it is not the first time that some systems are characterized by rather low S_0^2 values.[88,89,94] Even more importantly is the fact that the optimized S_0^2 values obtained for all the parent systems investigated in this study consistently lie in the $0.43-0.57$ interval, see Table 1. The values reported for the $SrCoO_{2.5}$ case have not to be considered because the models used were not able to reproduce the

structure, vide infra. Summarizing, the quality of the fits performed perovskite structures using a very simple model (Figure 4), and the meaningful values of the optimized parameters (Table 1) testifie that $SrCoO_{3.0}$ (i.e., the final product of the in situ oxidation of $SrCoO_{2.5}$) and the model $SrFeO_{3.0}$ compound have actually the expected structure.

The same effect holds also for the final product of the in situ oxidation of $SrFeO_{2.5}$, named $SrFeO_{3.0-\delta}$, that we already know did not reach the complete oxidation, see Figure 3a. Indeed, comparing the optimized parameters obtained for $SrFeO_{3.0-\delta}$ and $SrFeO_{3.0}$ samples, the main differences lies in a lower value of S_0^2 (by 4%) and a higher value of σ_1^2 (by 20%). The fitting procedure was able to account for the smaller intensity of the EXAFS oscillation of sample $SrFeO_{3.0-\delta}$ just by acting on S_0^2 and σ_1^2 parameters. This means that without the collection of the reference spectrum of $SrFeO_{3.0}$ model sample we would have been unable to prove that in the in situ electrochemical experiment the final oxidation state was not reached. It also means that the standard EXAFS analysis fails in determining whether the final sample exhibits a uniform $SrFeO_{3.0-\delta}$ phase or it represents the combination of the fully oxidized $SrFeO_{3.0}$ phase plus a parasitic one.

Moving from $SrFeO_{3.0}$ to $SrFeO_{2.5}$ the goodness factor of the simple 4-parameter model increases from 0.041 to 0.135. This is an expected behavior, because the adopted model is not able to fully take into account the complexity of the Brownmillerite structure. Just looking to the first shell Fe–O distances, the two Fe sites exhibit a broad distribution as nine different distances are present in the $1.8-2.2$ Å range.[25] In any case, all of the most important contributions coming from experimental data were represented quite well by the fitted curve, as shown in Figure 4. In this particular case only the contributions from O_h (0.5 weighted) and $T_d(Pnma)$ (0.5 weighted) Fe sites were employed to reproduce experimental behavior. Nevertheless this choice does not directly allow us to assign the $Pnma$ structure to $SrFeO_{2.5}$ because the same fitting procedure using O_h (0.5 weight) and $T_d(I2mb)$ (0.5 weight) Fe sites gave results similar to those shown in Table 1.

The fit of $SrCoO_{2.5}$ compounds gave even more troubles. Indeed the fit using as model the O_h and $T_d(Pnma)$ environments, both weighted by factor 0.5, was not able to reproduce the
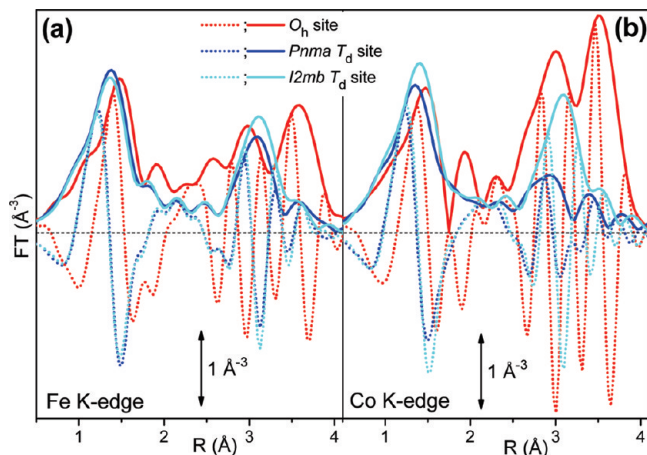
Figure 5. (a) Simulation of the k^2-weighted, phase uncorrected, FT ($2-12$ Å^{-1} interval) of the EXAFS signal arising from the local environment of Fe atoms (up to $R_{eff} = 4.2$ Å) hosted on O_h (red curves) and T_d sites of the SrFeO2.5 Brownmillerite structure. The latter being dependent on the adopted space group, the signals expected for both *Pnma* (blue curves) and *I2mb* (cyan curves) symmetries have been computed. The FT was performed in the $2-12$ Å^{-1} k-interval. (b) As in part a for the SrCoO2.5 Brownmillerite structure. In all cases $\Delta E_0 = 0$ eV; $S_0^2 = 1$; $\alpha = 0$; and $\sigma_1^2 = 0.003$ Å^2.

experimental spectrum, see Figure 4 ($R_{factor} = 0.285$). An even worst result (not reported) has been obtained using as model O_h (0.5 weighted) and T_d(*I2mb*) (0.5 weighted) resulting in an R_{factor} as high 0.458.

To understand why the same fitting procedure was able to reproduce quite satisfactorily the SrFeO2.5 data while it failed for the SrCoO2.5 case, a deeper discussion is needed. Figure 5 reports the simulation of the expected EXAFS signals (in R-space, k^2-weighted) for the local environment of Fe, part a, and Co, part b, when hosted in O_h (red curves) and T_d sites. The latter being dependent on the adopted space group, the signals expected for both *Pnma* (blue curves) and *I2mb* (cyan curves) symmetries have been computed. As for both SrFeO2.5 and SrCoO2.5 cases, the differences between O_h and T_d environments around absorber are evident, the same does not work when contributions from T_d sites with different structures are considered.

Looking at the SrFeO2.5 case, two important remarks are worth noting: (i) in the local environment of T_d sites both *Pnma* and *I2mb* symmetries results in an almost equivalent simulated EXAFS signal, with the same phase and just a slightly different amplitude (compare blue and cyan curves). (ii) In the $2.8-3.6$ Å interval O_h and T_d signals are almost totally out of phase. This latter point explains the important increase of the EXAFS signal in the $2.8-3.6$ Å region observed during the in situ

oxidation reaction 1, see Figure 2b: oxygen intercalation causes progressive transformation of the fraction of iron species hosted in T_d sites (50% at the beginning) into species in O_h symmetry, so causing the progressive disappearance of the destructive interference between O_h and T_d signals. The former point explains why the fits performed using *Pnma* and *I2mb* symmetries for describing the local environment of Fe in T_d sites gave basically the same result (Table 1). This also implies that our EXAFS spectrum is unable to contribute to the living debate on the actual space group of the SrFeO2.5 Brownmillerite structure.

The situation is very different for the SrCoO2.5 case, because here the signal seen for Co hosted in T_d sites is significantly different when *Pnma* or *I2mb* symmetries are assumed. Then in this case a EXAFS would, in principle, allow us to discriminate among the two space groups, but both approaches failed. As discussed in section 3, for Brownmillerite structures the choose of *Pnma*, *I2mb*, or *Imma* space groups is not always straightforward,[3] and this is relevant, because this choice can influence the EXAFS fit. Not considered in the fits reported in Table 1 was the even more complex case of *Imma*, space group, that can bee considered as a coherent mixture of the other two *Pnma* and *I2mb* space groups. This means that the Co average environment in the *Imma* space group can be modeled as a superimposition of 50% of O_h, x50% of T_d *Pnma* and $(1 - x)$50% of T_d *I2mb* contributions.

Before starting a fit based on the superimposition of three different local environments, some simplifications are required. The first one concerns the first shell Co–O contribution that, according to crystallographic data, is expected to be split into nine different contributions in the $1.81-2.26$ Å range. Because of the spatial resolution limitation and in agreement with our previous experience with similar systems,[88–93] EXAFS can not refine such a fine distributions of distances or the same scattering atom. It will simply optimize one (two) distance(s) and considering the distance distribution as a systematic increase of the Debye–Waller factor, whose value arises from the combination of factors of thermal and static origins. We thus first tried to optimize the first shell signal only with a single and a double Co–O shell model, as summarized in Table 2. A single Co–O shell fit is able to satisfactorily account for the experimental data, resulting in a R_{factor} as low as 0.004, with acceptable correlations among optimized parameters. The addition of a second independent Co–O2 distance was not necessary, as highlighted by the fact that its inclusion produced an near-zero value of the corresponding S_0^2 parameter and no further improvement of R_{factor} and correlations, while the optimized parameters for the first Co–O1 distance are compatible with those obtained from the one shell fit within the error

TABLE 2: Report of the Most Important Parameter Obtained by Fitting the First Shell Contribution of SrCoO2.5 with an Increasing Number of Single Co–O Distances[a]

	window (Å)	Ni/Nv	N S_0^2	ΔE_0 (eV)	R_{Co-O} (Å)	σ^2 (Å^2)	R_{factor}	correlations
			Fit of First Shell with a Single Co–O Contribution					
Co–O	0.9–2.30	7.77/4	1.93 ± 0.11	-6 ± 1	1.843 ± 0.005	0.0028 ± 0.0007	0.0041	S_0^2-$\sigma^2 = 0.82$
								ΔE_0-$\Delta R = 0.81$
			Fit of First Shell with Two SS Co–O Contributions					
Co–O1			1.95 ± 0.21		1.86 ± 0.02	0.0029 ± 0.001		$S_0^2$2-$\sigma^2$2 $= 0.86$
Co–O2	0.9–2.3	7.77/7	0.1 ± 0.2	-6.0 ± 1.5	2.01 ± 0.3	-0.003 ± 0.020	0.0024	ΔE_0-$\Delta R = 0.83$
								$S_0^2$1-$\sigma^2$1 $= -0.82$

[a] The values of N and R_{factor} points out directly if the addition of a further Co–O distance has its importance in reproducing experimental data. Resulting parameter from Co–O2 contribution highlight that we are able to fit reasonably whole first shell with a single Co–O distance.

TABLE 3: Summary of the Parameters Optimized in the EXAFS Fit of the Starting SrCoO$_{2.5}$ Brownmillerite Phase^a

Site or 1st shell	ΔE_0 (eV)	NS$_0^2$ or S$_0^2$	R$_{Co-O}$ (Å)	α	σ^2 or σ_1^2 (Å^2)	R$_{factor}$
Co−O	−4 ± 1	1.9 ± 0.1	1.850 ± 0.006	-	0.0027 ± 0.0009	0.020
O$_h$		0.280 ± 0.002	-	0	0.0052	
T$_d$(Pnma)		0.14	-			
T$_d$(I2mb)		0.14	-			

^{a} Fit was performed in *R* space (from 1.0 to 4.2 Å), on the k^2-weighted FT of the $\chi(k)$ function transformed in the $\Delta k = 2-12$ Å^{-1}, resulting in a number of independent parameters $N > 20$. For this brownmillerite O$_h$, T$_d$(Pnma), and T$_d$(I2mb) contributions can be separated, as shown in Figure 5, and in this case were weighted by 50%, 25%, and 25% values, respectively. Non-optimized parameters can be recognized by the absence of the corresponding error bar. Fits run over only 6 independent parameters. See Figure 6 for appreciating the quality of the fits in *R*-space.
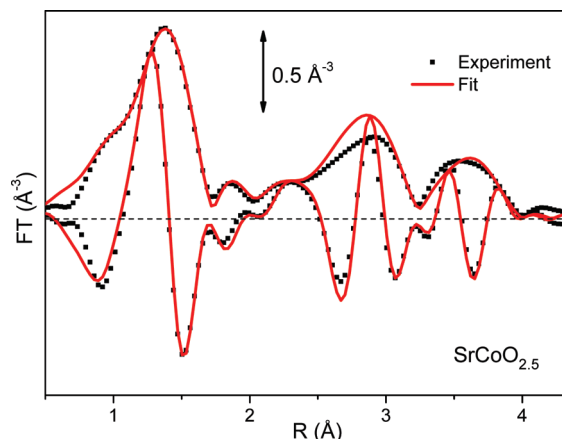

Figure 6. Graphical representation of the six-parameter fit on SrCoO$_{2.5}$ reported in Table 3. Fit was performed in *R*-space in the 1.0−4.2 Å range. Both |FT| and *Imm*(FT) are shown for experimental data (black scattered squares) and fit (red curve).

bars. This finding testifies that in the SrCoO$_{2.5}$ case we are unable to characterize the Co nearest neighborhoods disorder.

We can now proceed to the definitive fit for the SrCoO$_{2.5}$ sample. The fit uses the same ΔE_0 for all paths. The first shell Co−O is optimized with three additional parameters: N S$_0^2$, R$_{Co-O}$, and σ^2. The remaining higher shells SS and MS paths were optimized using a common S$_0^2$ amplitude factor weighted by fixed factors of 0.5, 0.25, and 0.25 for O$_h$, T$_d$ Pnma, and T$_d$ I2mb environments, respectively. The parameters α and σ_1^2 have been fixed to 0 and to the value optimized for the SrCoO$_{3.0}$ compound, respectively. Table 3 shows the optimized values of the four-parameter fit performed. The quality of the obtained fit can be appreciated both by R$_{factor}$ inspection and Figure 6 shows the comparison of |FT| and *Imm*(FT) between fit and experimental data.

Summarizing, the present EXAFS study proves that *Pnma* and *I2mb* space groups are, by far, not able to reproduced the average local environment of Co in SrCoO$_{2.5}$ Brownmillerite phase that can however be reconstructed, using a simple four-parameter fit assuming the disordered *Imma* space group. We are so able to confirm that the starting phases of both in situ oxidation experiments reported in Figures 2 and 3, well, corresponds to SrFeO$_{2.5}$ and SrCoO$_{2.5}$ compounds. The final spectrum of the electrochemical experiment at the Co K-edge is actually SrCoO$_{3.0}$, as expected.

4.1.2. Reconstruction of the Whole Set of Spectra As Linear Combination of the Starting and Final Phases. Figure 7 reports the results of the fit performed on the linear combination between starting (labeled "Red") and final (labeled "Ox") phases, for the Fe and Co K-edges data sets, parts a and b, respectively. In both cases fit were performed both in the XANES region (black scattered symbols) and in the EXAFS one (red scattered symbols). The squares represents the x_i^{Red} fraction of starting phase, while the stars describe the y_i^{Ox} fraction of the final phase, see eqs 2 and 3. It is interesting that a general accordance between the XANES and EXAFS results is present all along the reaction path for both SrFeO$_{2.5-x}$ and SrCoO$_{2.5-x}$ systems. Furthermore, once the edge position of ending spectra was overimposed "ad hoc" along the ordinate axis to fit together with the corresponding y_i^{Ox} scattered stars, the agreement of oxidation state respect to the phase fraction during reaction path is even more pronounced.

It is well known that transition metals hosted in a perovskite-type structure exhibit an unusual high valence state as (IV).[3] So, starting from a valence state of (III) in the Brownmillerite SrMO$_{2.5}$ phase, the oxidation reaction could drive a formal gradual M(III) → M(IV) transformation.[3,25] Nevertheless, for both experiments, the resulting valence state shift is not linear (Figure 7), to a different extent, a fact that is not associated
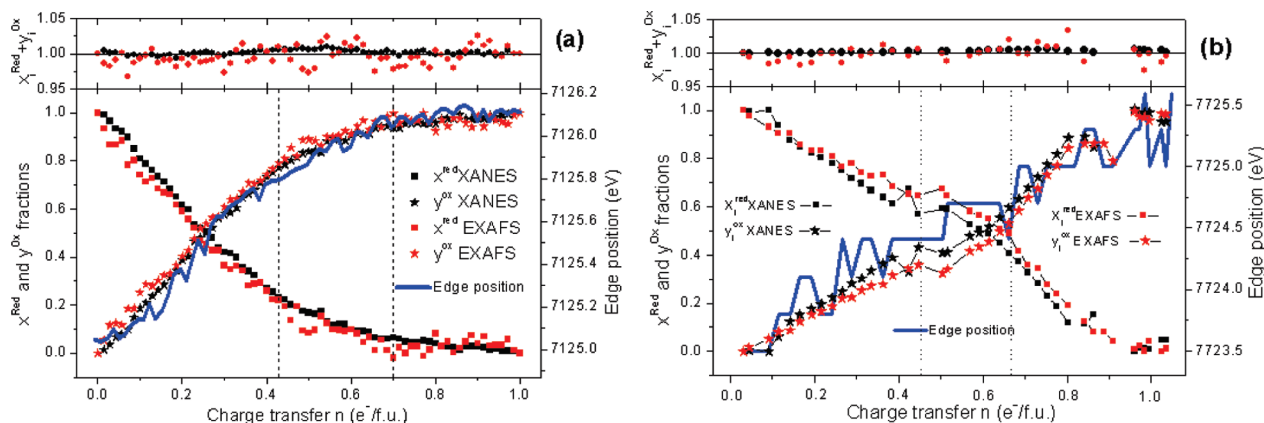

Figure 7. Left axis: evaluation of the reduced (square symbols) and oxidized (star symbols) phases as obtained from the XANES (black) and EXAFS (red) data. Right axis: shift of the edge position (blue line). Top part: sum of the reduced and oxidized fractions as obtained from XANES (black) and EXAFS (red) data. Part a refers to the Fe K-edge data set and part b to the Co one.

with the constant charge transfer imposed in the electrolytic cell formally described in eq 1. In the Fe case the deviation from linearity is quite large, and the valence vs n slope can be in principle described by three subregions. (i) The first one, $0 < n < 0.43$ e$^-$/f.u., exhibits a linear behavior, and it is associated with a parallel step linear progress of the oxidation state of Fe cations. (ii) The $0.43 < x < 0.7$ e$^-$/f.u. one presents a lightly parabolic increase that finally, (iii) above $x > 0.7$, reaches asymptotically a plateau, suggesting that saturation has been obtained. This saturation, after a charge transfer of only 0.7 e$^-$/f.u., is an unexpected finding if one has in mind eq 1. This mean that something has altered the general expected ideal behavior, as already pointed out when comparison between the final product of the in situ oxidation reaction (sample named SrFeO$_{3.0-\delta}$) has been compared with the model SrFeO$_{3.0}$ compound, see the XANES spectra reported in Figure 3a and discussion on the EXAFS data analysis (Table 2). A plausible explanation for this aspect is that the SrFeO$_{2.5}$ starting material has not reacted completely and the final product is a substoichiometric SrFeO$_{3-\delta}$ phase. Anyhow, it is also possible that during the reaction an unexpected product that does not concur in the electrochemical cycle had grown. A clarification of this aspect will be discussed later in this paper. Moving on to the Co case, three regions with different behaviors are present, as already extensively discussed elsewhere:[3] (i) $0 < n < 0.43$ e$^-$/f.u. presents a linear evolution, (ii) $0.45 < n < 0.65$ e$^-$/f.u. where the system seems almost unchanged, and (iii) $0.65 < n < 1$ e$^-$/f.u. with a steep linear increase with a slope almost twice the one present in the first region.

Comparing the two reaction pathways (see Figure 7), we immediately realize that the electrochemical reaction proceeds differently for the two systems. In fact, SrFeO$_{2.5}$, transforms to SrFeO$_{3.0}$ with a exponential saturation behavior as representing a random filling of oxygen vacancies that starts fast and then slows down until completion of sites at disposition. This scheme is supported by the fact that no ordered intermediate phase has been found by diffraction method during the in situ XRPD study by Nemudry et al.[25] Furthermore the unstructured continuum reaction scheme found in the Fe case is very different from the Co one. In this latter case, indeed, the inflection point among different linear oxidation regions coincides with oxygen stoichiometries of SrCoO$_{2.75}$ and SrCoO$_{2.875}$, which are known to be ordered intermediates, as evidenced in the in situ neutron powder diffraction study by Le Toquin et al.[3] This fact obliges us to choose a more sophisticated analysis technique to have the possibility of recognizing intermediates in the Fe case experiment, like PCA.

4.2. Principal Component Analysis. As discussed in section 2.3, PCA[38−42] is a powerful way to analyze a set of XAFS data, as alternative to the linear combination of standards. To gain the maximum of degree of freedom, PCA has to be applied to the whole range of data acquired during the reaction. This procedure was applied to both normalized XANES spectra and EXAFS oscillations in order to verify in parallel if changes in electronic configuration (preferentially probed by the former) were in accordance with local structure modifications (probed by EXAFS).

4.2.1. Fe Case. Decomposition of the obtained N spectra into principal components represent the first step of the analysis. In this way a set of N abstract components (vectors) are obtained and the first five of these components (those associated with the largest eigenvalues) were depicted in Figure 8b for both XANES and EXAFS data sets. The weight of each one of this eigenvectors is contained in its respective eigenvalue, shown
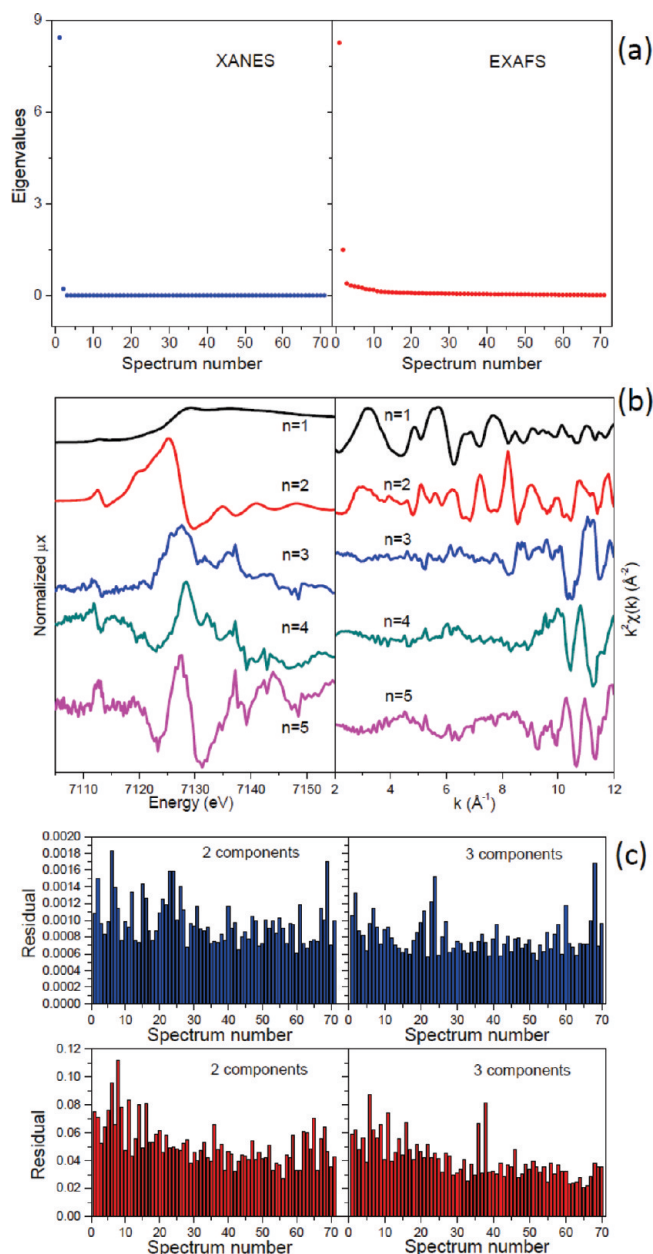

Figure 8. PCA analysis of the whole set of data of SrFeO$_{2.5+x}$ ($0 \leq x < 5$) oxidation reaction. (a) Abstract component obtained by the set of data: Principal components are those with higher eigenvalues. Inflection point divide components containing system information from noise. The five most intense eigenvalues are (8.423, 0.213, 0.005, 0.004, and 0.002) and (8.245, 1.493, 0.391, 0.318, and 0.297) for the XANES and EXAFS data sets, respectively. (b) Plot of the five most important components both for XANES and EXAFS regions (to have the actual weight, each eigenfunction has to be multiplied by its eigenvalue). (c) Calculated residual obtained using two or three principal components, on XANES spectra (blue bars) and EXAFS one (red bars), respectively.

in Figure 8a for XANES and EXAFS parts (blue and red scattered symbols, respectively). Then, the first eigenvector will contribute most to the representation of the whole set of data, the second in a major extent, and so on until a certain n_i value for which components start to reproduce mostly statistical noise. The minimum number n_i of the principal components which all data can be reliably represented may be obtained using a screen test, by finding the point where the slope of the eigenvalues in Figure 8a changes as a function of the number of components. For the case of XANES representation, it is evident that already the third component does not contribute to
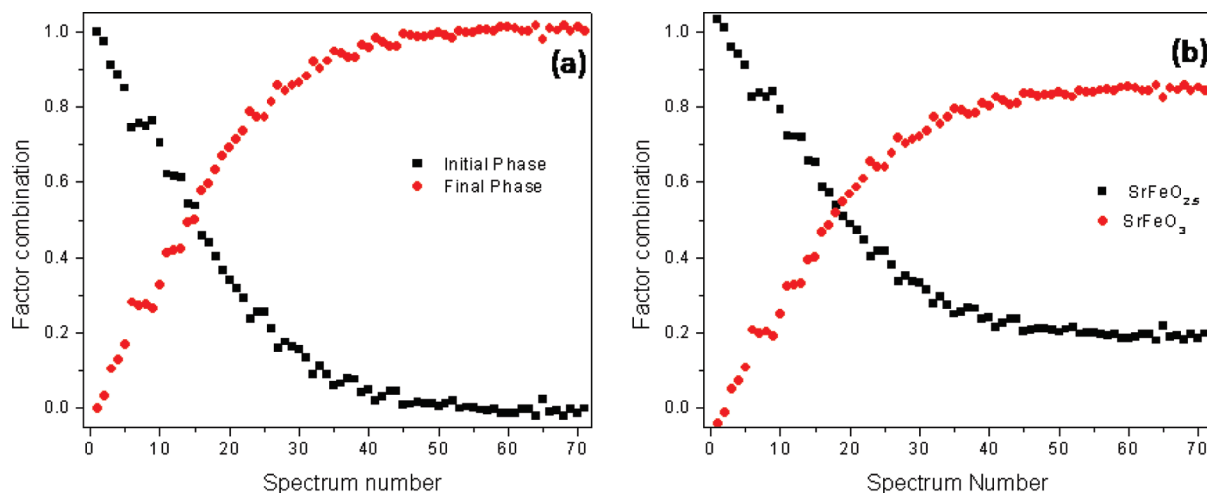
1320 *J. Phys. Chem. C, Vol. 115, No. 4, 2011*

Piovano et al.

Figure 9. Linear combination fit on $SrFeO_{2.5+x}$ system obtained from PCA. Part (a): combination between first and last spectra (samples named $SrFeO_{2.5}$ and $SrFeO_{3.0-\delta}$) showing same behavior as that reported in Figure 7a. Part (b): combination between the first spectrum $SrFeO_{2.5}$ and $SrFeO_3$ model compound, revealing the exactness of stoichiometry of starting sample, but not of final one. Last spectrum has a 20% contribution of a Fe(III) extra phase.

the signal (its eigenvalue is almost 0). For the EXAFS case, such determination is not straightforward. A visual inspection of EXAFS eigenfunctions for $n_i = 3-5$ (Figure 8b) points out that their contribution is significant in the $9-12$ Å^{-1} k-range only. Being the real data k^2-weighted, these vectors represent the amplified noise at high k values, where signal-to-noise ratio is lower. To resolve the doubt, it is possible to compute the residual, i.e., the difference between the combination of principal components with respect to the real data, in both cases. Results are plotted in Figure 8c for both XANES and EXAFS data (blue and red bars, respectively) and shows that the use of two or three principal components does not affect the overall trend of residuals. So it is clarified that the overall reaction can be represented by only two important components for both experiments.

It is evident that in cases where the PCA approach highlights the presence of three components, an intermediate phase must be present. However in cases similar to the present one, where only two components are clearly present, the presence of an intermediate phase can not be fully discarded. The reason why one phase may escape the PCA analysis can be explained in different ways: (i) two of the three phases always have a constant ratio along the whole reaction. This is the case of A $\rightarrow$ xB + (1 $-$ x)C, and then each spectrum of the series can be reproduced as combination of the starting phase A and an abstract spectrum $D = x(B - C) + C$. In this case only fitting with correct standards of (A, B, and C phases) can give a solution. This is exactly the case of the presence of an extra phase, which may be not wanted (parasite), growing during the reaction with the same rate as the product phase. (ii) One of the phases we are searching is disordered. In this case it will contribute to the first shell EXAFS signal only, possibly characterized by a low intensity because of a large value of Debye–Waller factor of static origin. It could thus be very difficult to extract its weak contribution from a spectrum with intense contribution from a more ordered perovskite phase: the extra phase is present but hardly detectable. (iii) The reaction scheme is complex, presenting ordered intermediate phases (A $\rightarrow$ B $\rightarrow$ C $\rightarrow$ ... $\rightarrow$ Z). In this case, it would be better divide the reaction path in more subintervals, where the transformation is simpler and analyzing them one after the other independently [(A $\rightarrow$ B), (B $\rightarrow$ C), ... (Y $\rightarrow$ Z)] and then see if boundary condition are fulfilled.

After abstract component manipulation, it is possible to come back to the real representation by testing suitable standards, in order to rotate the principal component with respect to the reference spectra. So, a representation of the whole reaction in function of mixing fraction of standards is possible, and Figure 9 show the results of such rotations applying two different standard sets.

In the first case initial and final spectra are chosen as standards and the result of Figure 9a evidence that whole set of data can be reproduced as combination of initial and final phases: this results is identical to the one obtained in Figure 7a with the classical linear combination approach. Instead Figure 9b present the results when Brownmillerite and Perovskite pure phases are chosen as standards. The initial part of the reaction is almost unchanged, demonstrating, once again, the presence of pure $SrFeO_{2.5}$ phase as a starting material. Instead, things change for the final state, demonstrating that the final phase is not the pure cubic fully oxidized phase. Having only 2 components, this factor combination mix with final state a 20% of the initial one to minimize least-squares, but presence of an (unknown) extra-phase could improve the agreement. Moreover, if we take also into consideration that only two components are sufficient to reproduce both EXAFS and XANES signals, we can say that our results are well represented by overmentioned case (i).

Finally, our in situ EXAFS/XANES study supports the presence of a parasitic phase with Fe(III) valence that grows up in parallel with $SrFeO_{2.5} \rightarrow SrFeO_3$ transformation but that can not be oxidized. This conclusion is supported by the following evidence: (i) in the Nemudry's study,[25] some extra diffraction peaks were observed for the final oxidation product (around $2\theta \approx 30.2°$, $37.2°$, $42°$, $44°$, $51.7°$, etc.) which can not be attributed to the cubic $SrFeO_3$ phase (see Figure 2a of the quoted work), (ii) no ordered intermediate phases were found by X-ray diffraction techniques, (iii) our analysis is compatible with the presence of an extra contribution all along the oxidation process. So, at the end of the reaction, a major part of the sample has reached the fully oxidized phase ($SrFeO_3$, as supported by the goodness of fit in Figure 4 and Table 1) and a minor part was transformed in a structure containing trivalent iron. In this regard, it is worth noticing that the formation of iron hydroxide during the cyclic voltammetry of $SrFeO_{2.91}$ has already been evidenced by situ Mössbauer spectroscopy,[95] According to this

study, we hypothesize the formation of iron hydroxyde parasitic phase along the electrochemical oxidation of SrFeO$_{2.5}$. As this phase can not be further oxidized under the adopted conditions we are able to explain the limited charge transfer of the oxidation reaction not exceeding 0.7 e$^-$/f.u.

4.2.2. Co Case. PCA was applied for completeness also on Co K-edge experimental data. As expected, it came out that component decomposition did not add anything relevant to the classical linear combination of starting and final phases reported in Figure 7b. Indeed, in this case, as the linear combination represented data without significant errors and as the starting and final phases represented well the respective expected stoichiometries, we were able to extract all important information using standard analysis techniques and PCA represented a model independent way to validate already obtained results.

5. Conclusions

In conclusion, with the application of a complex fitting procedure of EXAFS data, the linear combination method, and principal component analysis applied to both EXAFS and XANES data, we were able to highlight the different behavior of SrFeO$_{2.5}$ and SrCOO$_{2.5}$ systems during in situ electrochemical oxidation reactions. The surprising discovery that for SrCoO$_{2.5}$ EXAFS contributions from tetrahedra hosted in *Pnma* and *I2mb* space groups were different allowed us to obtain an optimized fit by introducing a coherent mixture of *Pnma* and *I2mb* contributions, whereas attempts to simulate the experimental data using only one of the two contribution fails. This means that our study reports a strong proof, based on the average order around Co atoms that SrCoO$_{2.5}$ actually belongs to the *Imma* space group. This conclusion is that it is very difficult to obtain by diffraction techniques because of the long-range disorder inherent to a random orientation of Co tetrahedra.[3] The same finding could not be appreciated in the SrFeO$_{2.5}$ compound because, in that case, the expected EXAFS signals of Fe in T_d(*Pnma*) and T_d(*I2mb*) sites are very similar, showing almost the same phase and having just amplitude differences in the 10% range, a difference that can be easily been simulated just by a small variation of the Debye−Waller factor associated to the corresponding SS and MS paths.

For the SrCoO$_{2.5}$ case, the oxidation reaction produced, at the end, the full oxide SrCoO$_3$ perovskite. The reaction scheme was obtained directly using a simple linear combination method, and its different behavior during the reaction, subdivided in three regions, suggested the presence of the SrCoO$_{2.75}$ case SrCoO$_{2.875}$ ordered intermediates[3] that have been found even at a local level. Conversely, in the SrFeO$_{2.5}$ case we found that the oxidation reaction proceed with a exponential-type saturation mode without the presence of intermediate locally ordered phases. Even more, we assigned the fact that the reaction saturated after a charge transfer of 0.7 e$^-$/f.u. to the presence of a parasite phase that grows in parallel with the oxide one. Most probably this phase is the hydroxide one.[96] To elucidate definitively this aspect, neutron diffraction is the most proper technique and will be the core of the next study.

References and Notes

(1) Grunbaum, N.; Mogni, L.; Prado, F.; Caneiro, A. *J. Solid State Chem.* **2004**, *177*, 2350–2357.

(2) Kozhevnikov, V. L.; Leonidov, I. A.; Patrakeev, M. V.; Mitberg, E. B.; Poeppelmeier, K. R. *J. Solid State Chem.* **2001**, *158*, 320–326.

(3) Le Toquin, R.; Paulus, W.; Cousson, A.; Prestipino, C.; Lamberti, C. *J. Am. Chem. Soc.* **2006**, *128*, 13161–13174.

(4) Nemudry, A.; Goldberg, E. L.; Aguirre, M.; Alario-Franco, M. A. *Solid State Sci.* **2002**, *4*, 677–690.

(5) Patrakeev, M. V.; Leonidov, I. A.; Kozhevnikov, V. L.; Kharton, V. *Solid State Sci.* **2004**, *6*, 907–913.

(6) Deb, A.; Bergmann, U.; Cramer, S. P.; Cairns, E. J. *J. Electrochem. Soc.* **2007**, *154*, A534–A541.

(7) Deb, A.; Bergmann, U.; Cramer, S. P.; Cairns, E. J. *J. Appl. Phys.* **2005**, *97*, 063701.

(8) Haas, O.; Deb, A.; Cairns, E. J.; Wokaun, A. *J. Electrochem. Soc.* **2005**, *152*, A191–A196.

(9) Deb, A.; Bergmann, U.; Cairns, E. J.; Cramer, S. P. *J. Synchrot. Radiat.* **2004**, *11*, 497–504.

(10) Deb, A.; Bergmann, U.; Cairns, E. J.; Cramer, S. P. *J. Phys. Chem. B* **2004**, *108*, 7046–7049.

(11) Tu, H. Y.; Takeda, Y.; Imanishi, N.; Yamamoto, O. *Solid State Ion.* **1999**, *117*, 277–281.

(12) Ma, B.; Victory, N. I.; Balachandran, U.; Mitchell, B. J.; Richardson, J. W. *J. Am. Ceram. Soc.* **2002**, *85*, 2641–2645.

(13) Traversa, E. *Sens. Actuator B-Chem.* **1995**, *23*, 135–156.

(14) Zhang, S. J.; Eitel, R. E.; Randall, C. A.; Shrout, T. R.; Alberta, E. F. *Appl. Phys. Lett.* **2005**, *86*, 262904.

(15) Fergus, J. W. *Sens. Actuator B-Chem.* **2007**, *123*, 1169–1179.

(16) Korotcenkov, G.; Do Han, S.; Stetter, J. R. *Chem. Rev.* **2009**, *109*, 1402–1433.

(17) Rao, C. N. R.; Cheetham, A. K. *Adv. Mater.* **1997**, *9*, 1009–1017.

(18) Vente, J. F.; Haije, W. G.; Rak, Z. S. *J. Membr. Sci.* **2006**, *276*, 178–184.

(19) Wiik, K.; Aasland, S.; Hansen, H. L.; Tangen, I. L.; Odegard, R. *Solid State Ion.* **2002**, *152*, 675–680.

(20) Baiker, A.; Marti, P. E.; Keusch, P.; Fritsch, E.; Reller, A. *J. Catal.* **1994**, *146*, 268–276.

(21) Patzke, G. R.; Michailovski, A.; Krumeich, F.; Nesper, R.; Grunwaldt, J. D.; Baiker, A. *Chem. Mater.* **2004**, *16*, 1126–1134.

(22) Michailovski, A.; Grunwaldt, J. D.; Baiker, A.; Kiebach, R.; Bensch, W.; Patzke, G. R. *Angew. Chem.-Int. Ed.* **2005**, *44*, 5643–5647.

(23) Perez-Alonso, F. J.; Melian-Cabrera, I.; Granados, M. L.; Kapteijn, F.; Fierro, J. L. G. *J. Catal.* **2006**, *239*, 340–346.

(24) Yang, Y.; Sun, Y. B.; Jiang, Y. S. *Mater. Chem. Phys.* **2006**, *96*, 234–239.

(25) Nemudry, A.; Weiss, P.; Gainutdinov, I.; Boldyrev, V.; Schollhorn, R. *Chem. Mater.* **1998**, *10*, 2403–2411.

(26) Paulus, W.; Cousson, A.; Dhalenne, G.; Berthon, J.; Revcolevschi, A.; Hosoya, S.; Treutmann, W.; Heger, G.; Le Toquin, R. *Solid State Sci.* **2002**, *4*, 565–573.

(27) Tsujimoto, Y.; Tassel, C.; Hayashi, N.; Watanabe, T.; Kageyama, H.; Yoshimura, K.; Takano, M.; Ceretti, M.; Ritter, C.; Paulus, W. *Nature* **2007**, *450*, 1062–1068.

(28) Kageyama, H.; Watanabe, T.; Tsujimoto, Y.; Kitada, A.; Sumida, Y.; Kanamori, K.; Yoshimura, K.; Hayashi, N.; Muranaka, S.; Takano, M.; Ceretti, M.; Paulus, W.; Ritter, C.; Andre, G. *Angew. Chem.-Int. Ed.* **2008**, *47*, 5740–5745.

(29) Paulus, W.; Schober, H.; Eibl, S.; Johnson, M.; Berthier, T.; Hernandez, O.; Ceretti, M.; Plazanet, M.; Conder, K.; Lamberti, C. *J. Am. Chem. Soc.* **2008**, *130*, 16080–16085.

(30) Inoue, S.; Kawai, M.; Ichikawa, N.; Kageyama, H.; Paulus, W.; Shimakawa, Y. *Nat. Chem.* **2010**, *2*, 213–217.

(31) Goodenough, J. B.; Huang, Y. H. *J. Power Sources* **2007**, *173*, 1–10.

(32) Tapilin, V. M.; Cholach, A. R.; Bulgakov, N. N. *J. Phys. Chem. Solids* **2010**, *71*, 1581–1586.

(33) Hodges, J. P.; Short, S.; Jorgensen, J. D.; Xiong, X.; Dabrowski, B.; Mini, S. M.; Kimball, C. W. *J. Solid State Chem.* **2000**, *151*, 190–209.

(34) Filipponi, A.; Borowski, M.; Bowron, D. T.; Ansell, S.; Di Cicco, A.; De Panfilis, S.; Itie, J. P. *Rev. Sci. Instrum.* **2000**, *71*, 2422–2432.

(35) Lamberti, C.; Bordiga, S.; Bonino, F.; Prestipino, C.; Berlier, G.; Capello, L.; D'Acapito, F.; Xamena, F.; Zecchina, A. *Phys. Chem. Chem. Phys.* **2003**, *5*, 4502–4509.

(36) Ravel, B.; Newville, M. *J. Synchrot. Radiat.* **2005**, *12*, 537–541.

(37) Zabinsky, S. I.; Rehr, J. J.; Ankudinov, A.; Albers, R. C.; Eller, M. J. *Phys. Rev. B* **1995**, *52*, 2995–3009.

(38) Fernandez-Garcia, M.; Marquez Alvarez, C.; Haller, G. L. *J. Phys. Chem.* **1995**, *99*, 12565–12569.

(39) Wasserman, S. R. *J. Phys. IV* **1997**, *7*, 203–205.

(40) Beauchemin, S.; Hesterberg, D.; Beauchemin, M. *Soil Sci. Soc. Am. J.* **2002**, *66*, 83–91.

(41) Wang, Q.; Hanson, J. C.; Frenkel, A. I. *J. Chem. Phys.* **2008**, *129*, 234502.

(42) Haider, P.; Grunwaldt, J. D.; Seidel, R.; Baiker, A. *J. Catal.* **2007**, *250*, 313–323.

(43) Alonso, J. M.; Cortes-Gil, R.; Ruiz-Gonzalez, L.; Gonzalez-Calbet, J. M.; Hernando, A.; Vallet-Regi, M.; Davila, M. E.; Asensio, M. C. *Eur. J. Inorg. Chem.* **2007**, 3350–3355.

(44) Bardelli, F.; Meneghini, C.; Mobilio, S.; Ray, S.; Sarma, D. D. *J. Phys.-Condes. Matter* **2009**, *21*, 195502.

(45) Cesano, F.; Scarano, D.; Bertarione, S.; Bonino, F.; Damin, A.; Bordiga, S.; Prestipino, C.; Lamberti, C.; Zecchina, A. *J. Photochem. Photobiol. A-Chem.* **2008**, *196*, 143–153.

(46) Choy, J. H.; Kim, D. K.; Hwang, S. H.; Demazeau, G. *Phys. Rev. B* **1994**, *50*, 16631–16639.

(47) Choy, J. H.; Kim, D. K.; Hwang, S. H.; Demazeau, G.; Jung, D. Y. *J. Am. Chem. Soc.* **1995**, *117*, 8557–8566.

(48) Farges, F.; Brown, G. E.; Rehr, J. J. *Phys. Rev. B* **1997**, *56*, 1809–1819.

(49) Frenkel, A. I.; Wang, F. M.; Kelly, S.; Ingalls, R.; Haskel, D.; Stern, E. A.; Yacoby, Y. *Phys. Rev. B* **1997**, *56*, 10869–10877.

(50) Garcia, J.; Sanchez, M. C.; Subias, G.; Blasco, J. *J. Phys.-Condes. Matter* **2001**, *13*, 3229–3241.

(51) Giannici, F.; Longo, A.; Balerna, A.; Kreuer, K. D.; Martorana, A. *Chem. Mater.* **2009**, *21*, 2641–2649.

(52) Giannici, F.; Longo, A.; Balerna, A.; Martorana, A. *Chem. Mater.* **2009**, *21*, 597–603.

(53) Groppo, E.; Prestipino, C.; Lamberti, C.; Carboni, R.; Boscherini, F.; Luches, P.; Valeri, S.; D'Addato, S. *Phys. Rev. B* **2004**, *70*, 165408.

(54) Groppo, E.; Prestipino, C.; Lamberti, C.; Luches, P.; Giovanardi, C.; Boscherini, F. *J. Phys. Chem. B* **2003**, *107*, 4597–4606.

(55) Grosvenor, A. P.; Greedan, J. E. *J. Phys. Chem. C* **2009**, *113*, 11366–11372.

(56) Grosvenor, A. P.; Ramezanipour, F.; Derakhshan, S.; Maunders, C.; Botton, G. A.; Greedan, J. E. *J. Mater. Chem.* **2009**, *19*, 9213–9220.

(57) Jiao, F.; Harrison, A.; Jumas, J. C.; Chadwick, A. V.; Kockelmann, W.; Bruce, P. G. *J. Am. Chem. Soc.* **2006**, *128*, 5468–5474.

(58) Jupe, A. C.; Cockcroft, J. K.; Barnes, P.; Colston, S. L.; Sankar, G.; Hall, C. *J. Appl. Crystallogr.* **2001**, *34*, 55–61.

(59) Karvonen, L.; Valkeapaa, M.; Liu, R. S.; Chen, J. M.; Yamauchi, H.; Karppinen, M. *Chem. Mater.* **2010**, *22*, 70–76.

(60) Kim, S. J.; Lemaux, S.; Demazeau, G.; Kim, J. Y.; Choy, J. H. *J. Am. Chem. Soc.* **2001**, *123*, 10413–10414.

(61) Lamberti, C.; Groppo, E.; Prestipino, C.; Casassa, S.; Ferrari, A. M.; Pisani, C.; Giovanardi, C.; Luches, P.; Valeri, S.; Boscherini, F. *Phys. Rev. Lett.* **2003**, *91*, 046101.

(62) Lamberti, C.; Prestipino, C.; Bonino, F.; Capello, L.; Bordiga, S.; Spoto, G.; Zecchina, A.; Moreno, S. D.; Cremaschi, B.; Garilli, M.; Marsella, A.; Carmello, D.; Vidotto, S.; Leofanti, G. *Angew. Chem.-Int. Ed.* **2002**, *41*, 2341–2344.

(63) Longo, A.; Giannici, F.; Balerna, A.; Ingrao, C.; Deganello, F.; Martorana, A. *Chem. Mater.* **2006**, *18*, 5782–5788.

(64) Luches, P.; D'Addato, S.; Valeri, S.; Groppo, E.; Prestipino, C.; Lamberti, C.; Boscherini, F. *Phys. Rev. B* **2004**, *69*, 045412.

(65) Luches, P.; Groppo, E.; D'Addato, S.; Lamberti, C.; Prestipino, C.; Valeri, S.; Boscherini, F. *Surf. Sci.* **2004**, *566*, 84–88.

(66) Luches, P.; Groppo, E.; Prestipino, C.; Lamberti, C.; Giovanardi, C.; Boscherini, F. *Nucl. Instrum. Methods Phys. Res. Sect. B-Beam Interact. Mater. Atoms* **2003**, *200*, 371–375.

(67) Nakayama, M.; Usui, T.; Uchimoto, Y.; Wakihara, M.; Yamamoto, M. *J. Phys. Chem. B* **2005**, *109*, 4135–4143.

(68) Ra, W.; Nakayama, M.; Cho, W.; Wakihara, M.; Uchimoto, Y. *Phys. Chem. Chem. Phys.* **2006**, *8*, 882–889.

(69) Ravel, B.; Stern, E. A.; Vedrinskii, R. I.; Kraizman, V. *Ferroelectrics* **1998**, *206*, 407–430.

(70) Ressler, T.; Timpe, O.; Neisius, T.; Find, J.; Mestl, G.; Dieterle, M.; Schlogl, R. *J. Catal.* **2000**, *191*, 75–85.

(71) Saini, N. L.; Bianconi, A.; Oyanagi, H. *J. Phys. Soc. Jpn.* **2001**, *70*, 2092–2097.

(72) Saini, N. L.; Lanzara, A.; Bianconi, A.; Chou, F. C.; Johnston, D. C. *J. Phys. Soc. Jpn.* **1998**, *67*, 16–19.

(73) Stern, E. A.; Yacoby, Y. *J. Phys. Chem. Solids* **1996**, *57*, 1449–1455.

(74) Truccato, M.; Lamberti, C.; Prestipino, C.; Agostino, A. *Appl. Phys. Lett.* **2005**, *86*, 213116.

(75) Deb, A.; Ralph, J. M.; Cairns, E. J.; Bergmann, U. *Phys. Rev. B* **2006**, *73*, 115114.

(76) Deb, A.; Bergmann, U.; Cramer, S. P.; Cairns, E. J. *J. Appl. Phys.* **2006**, *99*, 063701.

(77) Prestipino, C.; Bordiga, S.; Lamberti, C.; Vidotto, S.; Garilli, M.; Cremaschi, B.; Marsella, A.; Leofanti, G.; Fisicaro, P.; Spoto, G.; Zecchina, A. *J. Phys. Chem. B* **2003**, *107*, 5022–5030.

(78) Muddada, N. B.; Olsbye, U.; Caccialupi, L.; Cavani, F.; Leofanti, G.; Gianolio, D.; Bordiga, S.; Lamberti, C. *Phys. Chem. Chem. Phys.* **2010**, *12*, 5605–5618.

(79) Muddada, N. B.; Olsbye, U.; Leofanti, G.; Gianolio, D.; Bonino, F.; Bordiga, S.; Fuglerud, T.; Vidotto, S.; Marsella, A.; Lamberti, C. *Dalton Trans.* **2010**, *39*, 8437–8449.

(80) Frenkel, A. I.; Kleifeld, O.; Wasserman, S. R.; Sagi, I. *J. Chem. Phys.* **2002**, *116*, 9449–9456.

(81) Wasserman, S. R.; Allen, P. G.; Shuh, D. K.; Bucher, J. J.; Edelstein, N. M. *J. Synchrot. Radiat.* **1999**, *6*, 284–286.

(82) Webb, S. M. *Phys. Scr.* **2005**, *T115*, 1011–1014.

(83) Bordiga, S.; Bonino, F.; Damin, A.; Lamberti, C. *Phys. Chem. Chem. Phys.* **2007**, *9*, 4854–4878.

(84) Wilke, M.; Farges, F.; Petit, P. E.; Brown, G. E.; Martin, F. *Am. Mineral.* **2001**, *86*, 714–730.

(85) Berlier, G.; Spoto, G.; Bordiga, S.; Ricchiardi, G.; Fisicaro, P.; Zecchina, A.; Rossetti, I.; Selli, E.; Forni, L.; Giamello, E.; Lamberti, C. *J. Catal.* **2002**, *208*, 64–82.

(86) Lamberti, C.; Bordiga, S.; Salvalaggio, M.; Spoto, G.; Zecchina, A.; Geobaldo, F.; Vlaic, G.; Bellatreccia, M. *J. Phys. Chem. B* **1997**, *101*, 344–360.

(87) Grunwaldt, J. D.; Caravati, M.; Hannemann, S.; Baiker, A. *Phys. Chem. Chem. Phys.* **2004**, *6*, 3037–3047.

(88) Estephane, J.; Groppo, E.; Damin, A.; Vitillo, J. G.; Gianolio, D.; Lamberti, C.; Bordiga, S.; Prestipino, C.; Nikitenko, S.; Quadrelli, E. A.; Taoufik, M.; Basset, J. M.; Zecchina, A. *J. Phys. Chem. C* **2009**, *113*, 7305–7315.

(89) Estephane, J.; Groppo, E.; Vitillo, J. G.; Damin, A.; Gianolio, D.; Lamberti, C.; Bordiga, S.; Quadrelli, E. A.; Basset, J. M.; Kervern, G.; Emsley, L.; Pintacuda, G.; Zecchina, A. *J. Phys. Chem. C* **2010**, *114*, 4451–4458.

(90) Bonino, F.; Chavan, S.; Vitillo, J. G.; Groppo, E.; Agostini, G.; Lamberti, C.; Dietzel, P. D. C.; Prestipino, C.; Bordiga, S. *Chem. Mater.* **2008**, *20*, 4957–4968.

(91) Chavan, S.; Vitillo, J. G.; Groppo, E.; Bonino, F.; Lamberti, C.; Dietzel, P. D. C.; Bordiga, S. *J. Phys. Chem. C* **2009**, *113*, 3292–3299.

(92) Chavan, S.; Bonino, F.; Vitillo, J. G.; Groppo, E.; Lamberti, C.; Dietzel, P. D. C.; Zecchina, A.; Bordiga, S. *Phys. Chem. Chem. Phys.* **2009**, *11*, 9811–9822.

(93) Bordiga, S.; Bonino, F.; Lillerud, K. P.; Lamberti, C. *Chem. Soc. Rev.* **2010**, *39*, 4885–4927.

(94) Gianolio, D.; Groppo, E.; Estephane, J.; Prestipino, C.; Nikitenko, S.; Zecchina, A.; Bordiga, S.; Taoufik, M.; Quadrelli, E. A.; Basset, J. M.; Lamberti, C. *J. Phys: Conf. Ser.* **2009**, *190*, 012140.

(95) Fierro, C.; Carbonio, R. E.; Scherson, D.; Yeager, E. B. *Electrochim. Acta* **1988**, *33*, 941–945.

(96) Berthier, T. Oxygen mobility in solid oxides at moderate temperature: Crystal Growth, Structure Analysis, Lattice Dynamics and Chemical Reactivity of (Ca, Sr)FeO$_{2.5+x}$ $0 \leq x \leq 0.5$; PhD in Materials Science; University of Turin (I) & University of Rennes-1, 2007.